1
Fusion Research

This chapter provides a brief overview of the physics basis and the aims of fusion research and of the types of experimental devices used for the magnetic confinement of hot plasmas. It sketches the geometry in which plasma diagnostic systems are operated and gives one possibility to order and categorize, from an experimental viewpoint, the large number of diagnostic systems in use at modern fusion experiments.

The diagnostic systems collect the experimental data, thus providing the basis for fusion research aiming at understanding the complex behavior of the hot magnetized plasma, which is considered as necessary for the development of the optimum confinement device and optimal scenarios for a burning fusion plasma.

1.1
Reaction Scheme

Fusion research is the long-term effort to develop an almost inexhaustible energy source, based on fusion reactions among light atomic nuclei similar to those present in the interior of stars. The physics basis for these burning processes is the fact that the binding energy per nucleon in an atomic nucleus is a function of its mass number A_m, increasing by about one order of magnitude from about 1 MeV per nucleon at $A_m = 2$, deuterium (^{2}D), to the maximum at $A_m = 56$, iron (^{56}Fe). Beyond iron, the binding energy per nucleon decreases. Therefore, energy can be gained by the fusion of light elements as well as by the fission of heavier ones. The fusion-based energy production is connected with the formation of heavier elements. The stars create in this way the elements beyond hydrogen and helium. The young universe consisted of only light elements, about 75% hydrogen (^{1}H and ^{2}D), about 25% helium (^{4}He), and a very small amount of lithium (^{7}Li) and beryllium (^{9}Be). The first stars are formed out of this mixture. All elements with mass numbers up to 56 are produced by nuclear synthesis within the stars. The elements beyond are mainly produced by neutron capture and subsequent decay processes when the stars are collapsing in a supernova [1].

Taking the Sun as an example of a typical star in the stable, longest lasting period of its life, most of the power is generated by burning hydrogen into helium in a

Fusion Plasma Diagnostics with mm-Waves: An Introduction, First Edition.
Hans-Jürgen Hartfuß and Thomas Geist.
© 2013 Wiley-VCH Verlag GmbH & Co. KGaA. Published 2013 by Wiley-VCH Verlag GmbH & Co. KGaA.

COPYRIGHTED MATERIAL

process called proton–proton-chain (pp-chain). This process involves a three-step reaction: (i) two protons are combined to form first deuterium, $p(p, e^+\nu_e)d$; (ii) after this, the deuterium incorporates with another proton, forming helium-3, $d(p, \gamma)^3He$; (iii) and then two helium-3 nuclei are merged together, finally forming helium-4, $^3He(^3He, 2p)^4He$, releasing two protons [2]. Altogether, four protons are combined into one α-particle, the helium nucleus: $4p \rightarrow {}^4He + 2e^+ + 2\nu_e$. By almost 10^{38} fusion reactions per second, a mass of 567×10^9 kg hydrogen is burned into 563×10^9 kg of helium, releasing a total power of about 10^{26} W, equivalent to the mass loss of 4×10^9 kg each second. The generated fusion power of the Sun is dissipated mainly as electromagnetic radiation with a near-blackbody spectrum of 5800 K radiation temperature, corresponding to the physical temperature of the Sun's photosphere.

Energy production is concentrated in the very center of the Sun (<0.2 of the Sun radius) and it is taking place under conditions of extreme pressure (about 10^{16} Pa) and high temperature (1.5×10^7 K) caused by the contracting gravitational forces of the huge mass concentration.

The high temperature is necessary for the burning process to occur, as it is needed to overcome the repelling Coulomb forces between the equally charged ions.

The high kinetic energy enables the fusion partners to come close enough together (10^{-15} m) that the attracting strong but short-range nuclear forces are outbalancing the repelling Coulomb forces, combining the two into a stable heavier nucleus. The fusion power density P_{fus} generated depends on the densities n_1 and n_2 of the reaction partners, the energy W_{fus} released per reaction, and the strongly temperature-dependent velocity-averaged reaction rate coefficient $\langle\sigma v\rangle_v$,

$$P_{fus} = n_1 n_2 \langle\sigma v\rangle_v W_{fus} \tag{1.1}$$

Since weak interaction is involved in the first step of the pp-chain (e^+-decay), the rate coefficient is extremely small and the fusion power density in the Sun center is only of the order $100\,W\,m^{-3}$, despite the extreme density of reaction partners. Thus, the large total power released is attributable to the size of the Sun and not connected with a large reaction rate per volume.

Copying this reaction scheme for energy production on the Earth has therefore little chance of success. Fortunately, more promising reaction schemes exist. The one envisaged for controlled thermonuclear fusion on the Earth is the $d(t,n)\alpha$ reaction:

$$^2D + {}^3T \rightarrow {}^4He\,[3.5\,MeV] + {}^1n\,[14.1\,MeV] \tag{1.2}$$

It is characterized by a rate coefficient higher than that within the Sun by about 27 orders of magnitude, as shown in Figure 1.1.

However, the temperature needed is about 10^8 K, higher than the temperature in the Sun center by almost one order of magnitude. The reaction envisaged is the reaction between the hydrogen isotopes deuterium and tritium resulting in an α-particle (^4He) plus a neutron (^1n), releasing in total 17.59 MeV of energy. This energy is distributed as kinetic energy within the reaction products. Due

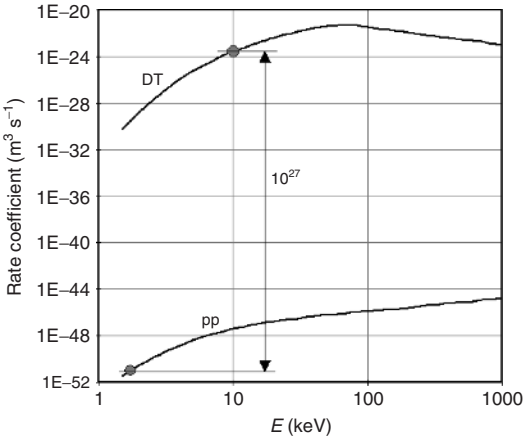

Figure 1.1 The velocity-averaged rate coefficients $\langle \sigma v \rangle$ for the pp-chain of the Sun at 15 million K and the DT-reaction at 100 million K envisaged for fusion energy production on the Earth differ by about 27 orders of magnitude.

to the conservation of momentum, it is distributed inversely proportional to their mass, $m_\alpha / m_n = W_n / W_\alpha$. The kinetic energies of the α-particle and the neutron are given in square brackets in Equation 1.2. Applying Equation 1.1 with typical densities of the reaction partners deuterium and tritium of modern fusion experiments, which are envisaged as well for the future fusion reactor, $n_D = n_T = 0.6 \times 10^{20}\ \mathrm{m}^{-3}$, with the rate coefficient $\langle \sigma v \rangle_v \approx 10^{-22}\ \mathrm{m}^2\ \mathrm{ms}^{-1}$ and the fusion energy per reaction, $W_{fus} = 2.8 \times 10^{-12}$ W s, the resulting power density shows promising $P_{fus} \approx 1\ \mathrm{MW\ m}^{-3}$.

While the fuel element deuterium is present in the oceans, the hydrogen isotope tritium is unstable, decaying into helium plus an electron and an electron neutrino, with a half-life of 12.3 years, according to

$$^3\mathrm{T} \rightarrow {}^4\mathrm{He} + \mathrm{e}^- [20\,\mathrm{keV}] + \nu_e \tag{1.3}$$

Thus, in the Earth's atmosphere, tritium is present only in very small quantities as a result of cosmic radiation interaction or imported with the solar wind. The estimated total equilibrium tritium mass in the atmosphere is only about 3 kg.

For large-scale industrial applications in a fusion power plant, tritium needs to be generated by neutron impact from lithium isotopes, according to

$$\begin{aligned} {}^6\mathrm{Li} + {}^1\mathrm{n} &\rightarrow {}^4\mathrm{He} + {}^3\mathrm{T} + 4.8\,\mathrm{MeV} \\ {}^7\mathrm{Li} + {}^1\mathrm{n} &\rightarrow {}^4\mathrm{He} + {}^3\mathrm{T} + {}^1\mathrm{n} - 2.5\,\mathrm{MeV} \end{aligned} \tag{1.4}$$

It is aimed at using fusion neutrons for that purpose. The fuel elements for a power plant based on the deuterium–tritium (DT) fusion reaction are therefore deuterium from the oceans and lithium occurring in the Earth's crust as well as in the oceans. They are almost uniformly distributed on the Earth. Along with the expected safety and environment-friendly properties, fusion power might therefore be called sustainable [3].

1.2 Magnetic Plasma Confinement

The hydrogen isotopes deuterium and tritium heated up to temperatures of the order 10^8 K are in the fully ionized plasma state. They must be confined without any material contact for a sufficiently long time that fusion reactions can occur at an adequate rate. The storage of the plasma in a vacuum chamber enclosed by a magnetic configuration with torus shape has turned out to be a promising confinement concept [4, 5]. Owing to the Lorentz force, $\vec{F} = q(\vec{v} \times \vec{B})$, a charged particle with charge q and velocity $\vec{v}$ can move freely along the magnetic field $\vec{B}$, but it is forced to gyrate around the $\vec{B}$-field line in the case where it has a velocity component perpendicular to it, in this way being bound to the field line. The toroidal $\vec{B}$-field applied in magnetic confinement devices is of the order of a few tesla, resulting in gyro-radii of several millimeters for the plasma ions and about a tenth of a millimeter for the electrons at the envisaged temperature. The pure torus field, however, has, in addition to curvature with radius $\vec{R}_c$, also a radially inward directed $\vec{B}$-field gradient $\vec{\nabla} B$.

Field curvature and field gradient cause charge-dependent particle drifts proportional to $\vec{B} \times \vec{R}_c$ and $\vec{B} \times \vec{\nabla} B$, respectively, leading to a separation of ions and electrons perpendicular to $\vec{B}$. The resulting electric field $\vec{E}$ gives rise to a radial outward drift of ions and electrons of the plasma proportional to $\vec{E} \times \vec{B}$. Thus, no force equilibrium is established. Since for particles on the inner edge of the torus, this outward drift is directed to the torus axis, and for those closer to the outer edge the drift direction is further out, the drift can be avoided on average by twisting the field lines to which the charged particles are bound. To accomplish this, it is necessary to superimpose a poloidal field $\vec{B}_\theta$ to the pure toroidal field $\vec{B}_\phi$, in order to cause the curvature – and the $\vec{\nabla} B$ – drift to cancel on average. Thus, the vertical charge separation is avoided, since short-circuited by the helical field lines (HFLs). The resulting net field is helical and might be expressed with unit vectors in toroidal and poloidal directions, $\hat{n}_\phi$ and $\hat{n}_\theta$, by $\vec{B} = \vec{B}_\phi \hat{n}_\phi + \vec{B}_\theta \hat{n}_\theta$ with $\vec{B}_\phi \gg \vec{B}_\theta$.

As depicted in Figure 1.2, the pitch of the resulting field line is determined by the ratio of the poloidal and toroidal field components and characterized by the rotational transform ι, which is the poloidal angle $\Delta\theta$ a field line is turned when performing a full revolution in toroidal direction $\Delta\phi = 2\pi$. The rotational transform is not constant along r. With $\iota_0 = \iota(r = 0)$, the value on the plasma axis, the dependence can be described by $\iota(r) = \iota_0 + (\partial\, \iota / \partial\, r)\delta r = \iota_0 + 2\pi \cdot S\delta r$, with the quantity S called shear.

The total field must be shaped and adjusted such that field lines never cross and that they form toroidal nested surfaces. Only in this case, particles confined to a field line lying further in would stay further in; those farther out would stay farther out. The existence of nested flux surfaces is a necessary condition for magnetic confinement.

The flux surfaces can be labelled by the magnetic flux they are enclosing. The innermost flux surface encloses zero volume. It is called magnetic axis. In the ideal case, field lines forming a magnetic surface never close on itself. Their rotational

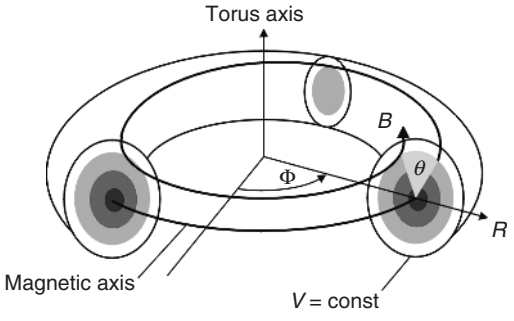

Figure 1.2 Magnetic confinement in torus geometry demands for twisted field lines that build up nested magnetic surfaces. The total $\vec{B}$-field is composed of a toroidal, B_Φ, and a smaller poloidal component, B_Θ. The nested magnetic surfaces show up as nested circles in a poloidal cross section, as indicated with the grey circles.

transform is therefore an irrational number. The radial range with nested magnetic surfaces is limited. A last closed magnetic surface exists. Farther out, field lines end on material boundaries, intersecting the vacuum chamber walls. Along those lines, particles leave the plasma, and no confinement is possible any longer. In this sense, the last closed surface defines the outer plasma edge in a magnetic confinement device. Two concepts have been developed differing in the way the field line twist is generated: the tokamak and the stellarator.

1.2.1 Tokamak

In the tokamak, a strong current of the order 10^6 A is induced in the toroidal plasma column generating the poloidal field, twisting the field lines and building up the nested magnetic surfaces as deemed necessary for confinement [4, 6].

The primary coil of this transformer-like arrangement, in which the plasma forms the secondary, is a solenoid coil along the center of the torus axis. To generate a constant plasma current, the flux in the primary solenoid coil must change at a constant rate to keep the induced toroidal loop voltage constant, which drives the plasma current. Since the swing in the primary transformer windings is finite, a classical/conventional tokamak is necessarily a pulsed device, although operation in modern devices can extend to several tens of minutes. The toroidal $\vec{B}$-field is produced by typically 12–20 planar equidistant discrete coils along the toroidal circumference. The radial position of the plasma is controlled by a vertical field generated by a pair of coils, one above and the other below the plane of the torus (Figure 1.3).

The torus geometry, as sketched in Figure 1.2 and Figure 1.6, is described by the major radius R_0 and the minor plasma radius a.

The radial coordinate r varies between the plasma axis at $r = 0$ and the plasma edge at the last closed flux surface at $r = a$. The ratio $A = R_0/a$ is called aspect ratio, typically lying between 2 and 6. The rotational transform expressed by the

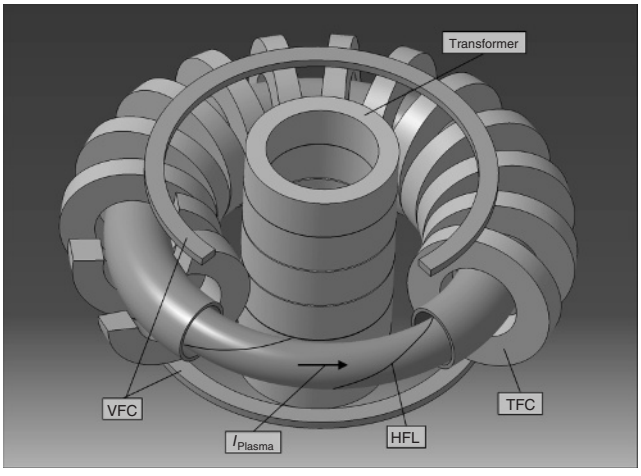

Figure 1.3 In a tokamak, the poloidal field component is generated by the strong plasma current I_p induced by magnetic flux changes in the central solenoid winding acting as primary winding of a transformer arrangement, and the toroidal plasma column forming the secondary one. The main toroidal field is built up by planar field coils (TFC). A pair of windings, the vertical field coils (VFC), one above and one below the torus plane, produce a vertical field that allows to shift the plasma column radially. A helical field line (HFL) demonstrates the twist as a result of the superposition of toroidal and poloidal field contributions.

field component ratio and the geometry parameters is $\iota/2\pi = R_0 B_\Theta / r B_\Phi$. The value $q = (\iota/2\pi)^{-1}$ is called safety factor.

The tokamak is axisymmetric, which means that arbitrary poloidal plasma cross sections are equivalent with respect to the plasma parameters. In cylindrical coordinates, r, Θ, Φ, with Θ the poloidal angle and Φ the toroidal angle, it is therefore sufficient to label any volume element of the plasma column by r, Θ. In cases where the plasma has circular cross section, the poloidal angle Θ, when considering physical quantities that are constant on flux surfaces, is negligible too. The toroidal $\vec{B}$-field, however, depends on the poloidal angle, $B_\phi = B_\phi(\Theta)$. In modern tokamaks, the poloidal plasma cross section is noncircular, typically vertically elongated, and D-shaped, allowing for equilibria at higher plasma currents [6].

1.2.2 Stellarator

In a stellarator, the whole confining field is produced by currents flowing outside the plasma. No induced plasma current is needed to build up the confining $\vec{B}$-field [4, 7]. Nevertheless, pressure-driven currents are present also in the stellarator; however, they are significantly smaller than the plasma current in tokamaks.

The coil system of a classical stellarator is composed of toroidal field coils similar to those of a tokamak, and pairs of helical windings with opposite currents within

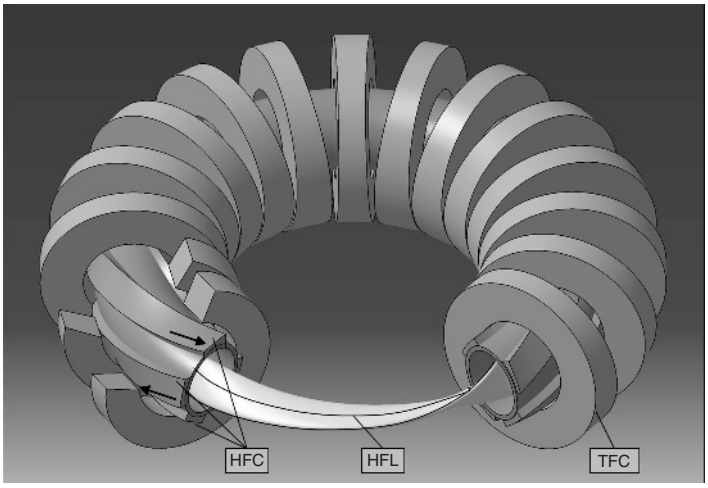

Figure 1.4 In the classical stellarator, the toroidal field is generated as in the tokamak by a set of planar toroidal field coils (TFC). The poloidal field component, however, is generated by currents exclusively outside the plasma. In the $l = 2$ stellarator, a pair of conductors with opposite currents are wound helically around the torus (HFC, helical field coil) generating the poloidal field component, resulting in helical field lines (HFL) necessary for plasma confinement. The plasma cross section is elliptical shaped, with the ellipse orientation varying with toroidal position.

the conductors of the pair, generating the rotational transform. Owing to the helical windings, the stellarator has no axial symmetry. With two pairs of helical windings ($l = 2$), the poloidal plasma cross section is elliptical; with three ($l = 3$), it is triangular, rotating around the plasma axis with toroidal coordinate Φ. The aspect ratio of stellarators is larger than that of tokamaks, typically around $R_0/a \approx 10$. Figure 1.4 shows a classical $l = 2$ stellarator.

Modern stellarators use modular nonplanar field coils that are able to generate arbitrary superpositions of classical stellarator fields, allowing for the optimization of the confining field configuration that is necessarily three-dimensional. It is optimized in various respects, considering the technical feasibility and, in particular, accounting for physics aspects, that is, improving the stability of the confined plasma as well as minimizing particle and energy transport across the magnetic surfaces [7].

Stellarators are intrinsically steady-state devices, and are highly advantageous in view of the applicability as power reactor [8]. However, the experimental database of tokamaks is by far larger. The next-step device, the International Thermonuclear Experimental Reactor (ITER), is therefore based on the tokamak principle [9].

1.2.3
Physics Issues of Magnetic Confinement

The hot plasma is confined in the magnetic torus configuration with nested magnetic surfaces. Assuming the electrons and ions of the plasma in Maxwellian

energy distributions, the plasma pressure p ($p = nk_B T$) is similar to the pressure of an ideal gas given by the product of particle density, in the plasma composed of electron and ion density, $n = n_e + n_i$, and the temperature $T = T_i = T_e$.

Stable operation is obtained if the plasma pressure is kept smaller than that of the magnetic field; the ratio of the two, the normalized plasma pressure, $\beta = 2\mu_0 p/B^2$, is therefore typically below 0.1. Since the plasma is confined to a bounded region, pressure gradients $\vec{\nabla} p$ evolve, balanced by the electromagnetic forces generated by currents with density $\vec{j}$ in the plasma and the external $\vec{B}$-field, $\vec{\nabla} p = \vec{j} \times \vec{B}$. The force balance implies $\vec{B} \cdot \vec{\nabla} p = 0$. Consequently, field lines lie in a constant-pressure surface and accordingly magnetic surfaces are surfaces of constant pressure.

Along with the pressure gradients, radially directed gradients of temperature and density exist, which are driving energy transport, $Q_E \propto -n\vec{\nabla} T$, and particle transport, $\Gamma_p \propto -\vec{\nabla} n$, across the flux surfaces from the hot and dense plasma center to its edge [10]. However, it turned out that collisional energy transport of the electrons is small compared to the transport driven by microturbulence in the plasma. Thus, small-scale turbulence of density and temperature correlated with electric and magnetic field fluctuations within the plasma is forming the main loss channel in magnetic confinement devices.

In addition to these main loss processes, energy is lost because of the emission of electromagnetic radiation from the plasma. The most effective radiation processes of the electrons are bremsstrahlung (due to their acceleration in the field of ions) and cyclotron radiation (due to the gyration around the field lines). Not fully ionized impurity ions in the plasma can give rise to atomic line emission after excitation by electron impact. Although the radiative losses due to the accelerated motion of the electrons are unavoidable, certain effort must be undertaken to keep the impurity level small enough that impurity radiation stays below a maximum acceptable level [11].

The necessary physics conditions of a fusion reactor based on the DT fusion reaction can be formulated by balancing the energy gain and loss processes. In a burning DT-plasma, the generated energetic α-particles stay confined. They heat the plasma when they slow down. Only their contribution enters the energy balance as gain, as the generated energetic neutrons leave the plasma, providing their kinetic energy to external systems.

Energy loss is caused by turbulent transport, diffusion, convection, and the radiative losses mentioned earlier. The various processes can be combined and globally be described by the quantity energy confinement time, τ_E. Its size is a measure of the energy insulation quality of the confinement device.

Positive energy balance is obtained in the case where the triple product of temperature (in energy units) and density of the reaction partners and the confinement time exceed a certain value called Lawson criterion: $nk_B T\tau_E \geq 5 \times 10^{21}\,\mathrm{keV\,s\,m^{-3}}$. With temperature T, with $k_B T \approx 10$ keV, and at particle densities of $10^{20}\ \mathrm{m}^{-3}$, the confinement time must amount to a few seconds [12].

The energy confinement time in modern laboratory fusion experiments is experimentally determined from the ratio of total stored energy W in the whole plasma volume, $W = \frac{3}{2}\int k_B(n_e T_e + n_i T_i)\,\mathrm{d}V$, to the net heating power $P_H = P_{ext} + P_\alpha - P_{rad}$, which is composed of external plasma heating with power P_{ext}, the

heating P_α by the fusion generated α-particles, and the radiation losses P_{rad} under steady-state conditions: $\tau_E = W/P_H$. Defining the Q-factor as the ratio of the fusion power output to the input power necessary to sustain the fusion reaction, the so-called break-even condition, $Q = 1$, corresponds to the minimum condition to sustain burning given by the Lawson criterion.

It turned out that the energy confinement time τ_E depends on a number of physical parameters as well as on the geometry of the confinement device. The energy confinement time improves with major and minor radii of the device, the plasma density, the main toroidal magnetic field, and the plasma current in the case of a tokamak, and it degrades with increasing heating power, recalling only the most important parameters. The dependencies explain the need for large devices to fulfill the Lawson condition. They are explored by deriving empirical scaling laws based upon the experimental results of many different devices of largely varying parameters (Figure 1.5).

Energy confinement time scaling is known accurate enough to allow for the extrapolation to reactor-like conditions, although the physics behind is still not understood in every detail. This is true especially for the turbulent transport. The triple product obtained in the most advanced fusion experiments is within a factor of 5 of that necessary in a fusion reactor [13].

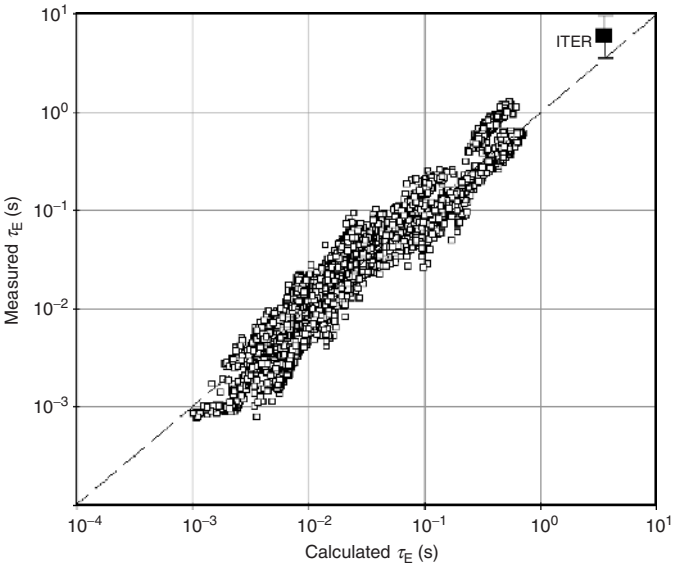

Figure 1.5 The energy confinement time τ_E is a global measure of the confinement quality of the device. It depends on machine parameters such as size and B-field as well as on the operation scenario, that is, heating power and plasma density. Comparison of experimental results from many different machines allows for the formulation of scaling laws that enables to extrapolate to next-step devices (here ITER), even if the physics behind it is still not understood in every detail. Data given in the figure are gained in both tokamak and stellarator experiments [13].

1.2.4 Plasma Heating

In a fusion reactor based on the DT-reaction, the plasma will be heated by the α-particles. However, DT-operation with fusion power gain has so far been conducted only in two major experiments, the Joint European Torus (JET) and the Tokamak Fusion Test Reactor (TFTR), with a strongly limited number of experiments [14, 15]. The typical fusion plasma experiments are conducted with hydrogen or deuterium or with mixtures of both. Therefore no internal energy gain from fusion reactions occurs; thus, heating is continuously necessary to study the plasma behavior at fusion-relevant temperatures and densities.

Basically three different heating schemes are possible and in use: (i) Joule or ohmic heating, (ii) particle heating by injected energetic particles, and (iii) heating by electromagnetic waves launched into the plasma.

Ohmic heating in tokamaks by the electron-carried induced plasma current I_p is based on the fact that the plasma column has a finite resistance R_p. Thus, the power $P_J = R_p I_p^2$ is dissipated. The resistance is caused by electron–ion collisions. Since the resistance decreases with increasing electron temperature, $R_p \propto T_e^{-3/2}$, the heating efficiency decreases as well. Ohmic heating is therefore restricted to the very start-up phase of tokamak operation. It is of course not used at all in stellarators.

The energy content of the plasma can efficiently be increased by neutral beam injection (NBI) of H- or D-particles with high energy (50–500 keV), which are ionized and slowed down and finally thermalized in collisional processes with the plasma electrons and ions, thus increasing the plasma energy content W. NBI heating affects the particle balance because, for example, some 10^{19} energetic particles with an energy of 100 keV need to be injected per second for generating 1 MW of heating power [16].

Wave heating is done at frequencies resonant with the gyration motion of electrons or ions called electron cyclotron resonance heating (ECRH) and correspondingly ion cyclotron resonance heating (ICRH). Since, at high temperatures, the plasma is almost collisionless, electromagnetic waves outside these resonances are not absorbed at all or not dissipated efficiently enough for heating purposes. Wave heating is therefore possible only if resonance conditions are fulfilled. The resonant frequencies depend on the B-field of the device they are applied, and are typically in the range 50–200 GHz in the case of ECRH, and 30–100 MHz for ICRH. Since the B-field varies with location within the plasma, resonance becomes a local phenomenon. Wave heating methods ECRH and ICRH allow therefore for localized heating of electrons and ions separately, as well as for current drive and shaping of the current profile, providing wide experimental fields of operation. The particle and wave heating methods are experimentally tested and technologically developed to provide heating powers of the order of several tens of megawatts even under steady-state conditions [17].

1.3 Plasma Diagnostic

Plasma diagnostic provides the experimental database for fusion research. Depending on the scientific problem and the related experimental program, a large number of plasma parameters needs to be known simultaneously. Among those parameters, the most important ones are the density and temperature of the plasma-forming constituents, electrons, ions, neutrals, and impurities, the total energy content of the plasma, the plasma pressure, plasma currents, local fields, plasma drift motions, and electromagnetic radiation of various origins. Most of them are time-dependent local quantities that must be measured with sufficient spatial and temporal resolutions.

The large variety of diagnostic methods applied originated from all areas of physics. Two general issues to be considered are redundancy and complementarity. Redundancy means, to determine the same physical quantity, different methods are to be applied to avoid or to detect systematic errors. Complementarity is necessary, on the one hand, to cover the full dynamic range of a certain plasma parameter that might range over orders of magnitude, demanding for different methods to cover that range. It is necessary, on the other hand, to provide information by one diagnostic system needed for the interpretation of another one, to complement one another.

These demands affect the various systems based on different physical methods applied, for example, to measure the electron temperature and density.

To optimally combine their results, integrated data analysis (IDA) is advantageous. In this attempt, the raw data of several diagnostic systems are combined to form a common physical picture as complete as possible, from which the quantity of interest is derived, instead of deriving it individually from each of the diagnostic systems, comparing and discussing possible discrepancies [18].

Generally, the physical quantities are time and space dependent. Owing to the fast equalization processes, however, they are generally constant on a flux surface. As we have seen, the pressure, as an equilibrium property, is constant on a flux surface. This means that measurements undertaken at different positions of the toroidal plasma are identical in the case where they are made at the same flux surface. Therefore, for comparison, the laboratory coordinates defining the measurements need to be transformed to flux coordinates or to the effective radial coordinate of an equivalent axisymmetric plasma with cylindrical cross section.

If not explicitly mentioned otherwise, we will assume that this is possible under the conditions discussed in this book. Figure 1.6 shows the geometry we are referring to with $R_0 \gg a$, thus treating the torus in the limit of a straight cylinder.

The only local coordinate will then be the radial position r, ranging from the plasma axis to the plasma edge, $0 \leq r \leq a$. To stay descriptively connected with the experimental arrangement, profiles are often given, despite they are symmetric in this representation, across the full plasma column, $-a \leq r \leq a$. Profile maxima, either peaked or broad, of the most important quantities (pressure, density, and temperature) are located in the plasma center near the axis, with the quantities

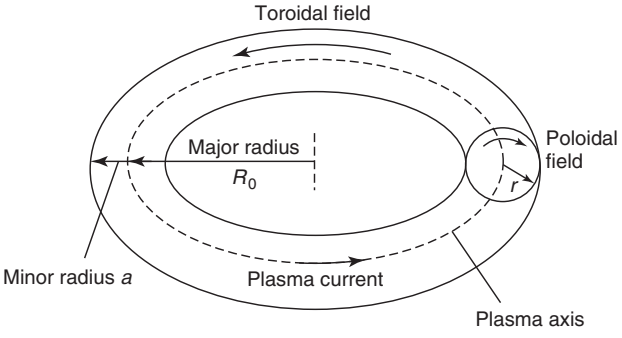

Figure 1.6 The geometry used to describe the plasma in the frame of this book. Axial symmetry is assumed with circular poloidal plasma cross section. Other symmetries can be transformed to this by comparison of the volumes enclosed by flux surfaces. In the geometry shown, the radial coordinate r is sufficient to describe density and temperature profiles of the confined plasma.

approaching zero at the edge. Typical scale lengths are of the order of centimeters (in large devices, tens of centimeters), which need to be resolved by the diagnostic systems. All quantities are time dependent, varying on a time scale of the order of the confinement time. Many diagnostic systems should be able to resolve the much faster magneto-hydrodynamic (MHD) phenomena, occurring on a millisecond time scale as well. Special fluctuation diagnostic systems dedicated to turbulence studies, however, need sub-microsecond time resolution.

1.3.1 Generic Arrangements

To avoid perturbation of the plasma by the measuring diagnostic instruments and to avoid destruction of their detectors, probing of the hot fusion plasma must be conducted without any material contact between the detection system and the plasma. The only exceptions are Langmuir probes applied for short time intervals at the less hot very plasma edge. All other diagnostic systems are either based on the analysis of waves or particles emitted by the plasma or involve passing waves or particle beams through the plasma and analyzing the result of their interaction with it.

From the experimental viewpoint, the large variety of different diagnostic systems present on modern fusion experiments can be arranged into four groups: composed of wave or particle diagnostics, and either active or passive.

In addition to these four groups, we have Langmuir probes and magnetic diagnostics, which do not fit unconstrained into that scheme. Probes either inject electrons into the plasma or extract them out of it. Magnetic diagnostics measure magnetic flux changes caused by the plasma diamagnetism as well as by induced and pressure-driven currents. Besides this more experimentally oriented ordering scheme, the variety of diagnostic systems can be distinguished with respect to the physical processes [19] or by the experimental methods involved [20]. Figures 1.7–1.11 show the generic arrangements for active and passive probing

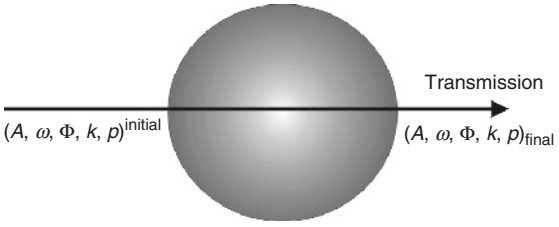

Figure 1.7 Active probing of the plasma by launching a wave and measuring changes in the wave's characterizing quantities amplitude, frequency, phase wave vector, and polarization state. Conclusions on the kind and strength of the plasma–wave interaction can be drawn, from which plasma parameters can be determined. The arrangement shown in this figure is used to measure changes in phase and polarization states of the wave in interferometry and polarimetry diagnostic systems (Section 1.3.1 and Section 1.3.2). The single chord arrangement gives line-integrated information. To obtain local information, multiple chords are needed.

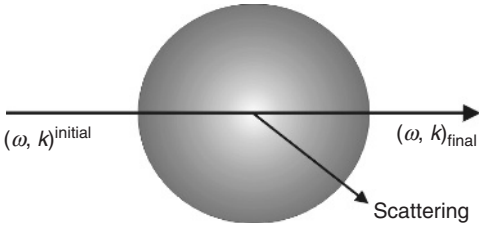

Figure 1.8 The electric field of the wave passing the plasma accelerates individual plasma electrons, thus becoming themselves emitters of electromagnetic radiation (Thomson scattering, Section 3.4). Since the scattering electrons are moving corresponding to their temperature, their emission is Doppler shifted with respect to the probing wave frequency. At fusion-relevant temperatures, the emission is relativistically blue-shifted, in addition. The width of the spectrum reflects the velocity distribution along the scattering vector. Depending on the scattering geometry and the wavelength of the primary wave, scattering is caused by individual electrons (incoherent scattering) or can as well be caused by collective action of the large number of electrons in a Debye cloud, reflecting the motion of the ions (coherent scattering).

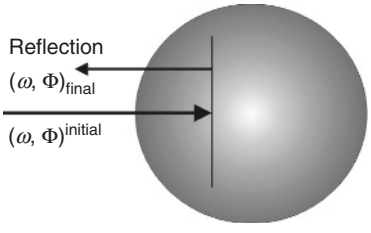

Figure 1.9 The wave launched into the plasma can be reflected back when reaching a cutoff layer where the refractive index approaches zero. The conditions are mainly determined by the space-dependent electron density in the plasma. By measuring the round trip phase delay of the wave in this RADAR-like arrangement, the location of the cutoff layer can be determined. Thus, local plasma parameters determining the wave cutoff can be derived with the method (Section 3.3).

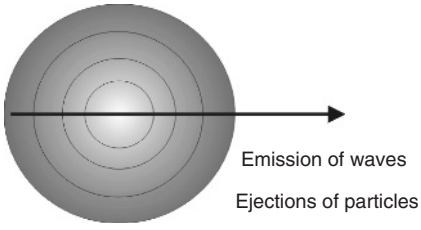

Figure 1.10 The plasma emits electromagnetic radiation in a wide spectral range extending from the gyration frequency of the ions at tens of megahertz to the X-ray region. Passive spectroscopy of the emission is the classical way to gain information about the plasma constitution and state. The physical mechanisms causing the emission range from gyration motion of the charged particles around the field lines and bremsstrahlung of the electrons in the fields of the ions to line emission of not fully ionized impurity atoms within the plasma. The presence and the concentration of the impurities can basically be derived from the line intensity. The line width of the emission is carrying information on the velocity distribution. All processes are strongly dependent on temperature and density of the plasma. Neutralized particles are leaving the plasma as well. These particles are recombined plasma ions undergoing charge exchange with neutral particles from the NBI heating system, or with neutrons from fusion reactions. All particles escaping from the plasma reflect the ion energy distribution in the plasma, which can be determined by measuring the energy distribution of the leaking particles.

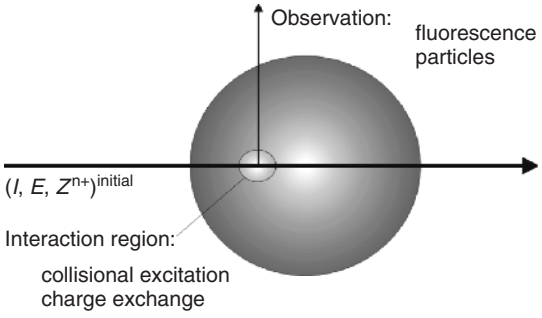

Figure 1.11 Atomic beams are injected into the plasma in arrangements of active particle probing diagnostics. The beam atoms are excited in electronic collisions. The subsequent emission is analyzed spectroscopically, giving local information on density and temperature within the plasma volume defined by the crossing of particle and observation beams. The neutral atomic beam also provides electrons for charge exchange processes with the plasma ions. Their broadened and shifted emission is carrying information on the ion velocity distribution.

Table 1.1 The table lists the standard diagnostic systems by dividing into active and passive systems, either probing with waves or with particles.

Passive diagnostics	Active diagnostics
Waves	**Waves**
Spectroscopy (IR, visible, UV, VUV, and X-ray)	Interferometry
Radiometry of electron cyclotron emission	Polarimetry
Bolometry of total radiation	Reflectometry
Thermography of wall surfaces	Scattering (incoherent and coherent)
Particles	**Particles**
CX neutral particle analysis	H-, He-, Li-beam, and emission after e^- impact
Detection of fusion products	CX recombination spectroscopy

VUV, vacuum ultraviolet; CX, charge exchange

with waves and particles and they briefly list the physics principle behind. Table 1.1 summarizes the standard diagnostic systems according to the experimentally oriented scheme, active or passive, wave or particle diagnostic systems.

1.3.2 Microwave Diagnostics

Microwave diagnostics, on which the book focuses, are active and passive wave diagnostic systems. They are operated in a range of frequencies where the refractive index of the magnetized plasma differs significantly from the vacuum value and/or where it shows largest variations with plasma parameters. The range depends on the electron density and on the $\vec{B}$-field, the first determining the plasma frequency ω_p, the frequency electrons are oscillating against the fixed ion background, and the second determining the frequency the electrons are gyrating around the field lines, the electron cyclotron frequency ω_c. Combinations of these two quantities determine almost exclusively the refractive index in the frequency range of interest. The influence of collisions and ion motion on it is negligible. In modern fusion experiments, the plasma and cyclotron frequencies, because of the densities at which the experiments are typically conducted, and because of the $\vec{B}$-fields they are operating in, are in the range 50–200 GHz, corresponding to wavelengths between 6 and 1.5 mm. Consequently, it is the millimeter-wavelength range in which microwave diagnostic systems are operated.

These systems probe the plasma dielectric properties by measuring the wave phase (interferometry) and polarization changes (polarimetry) when passing the plasma and probe the localization of cutoff layers by measuring time delays in radio detection and ranging RADAR-like schemes (reflectometry). Since wave–plasma interaction is governed by the electron component, all information obtained from millimeter-wave probing characterizes the plasma electrons. But, there is

one exception: the occurrence of wave scattering. Two different situations arise, depending on the scattering geometry and the probing wavelength: incoherent and coherent scattering. In the first case, scattering is accomplished by individual electrons; in the second case, it is scattered coherently by a large number of electrons attracted by a single ion within its Debye sphere. In the latter case, information on the ion velocity distribution and on the ion charge can be gained.

The plasma absorbs and emits electromagnetic radiation at the gyration frequency of the electrons and their harmonics. Measuring the intensity of this radiation gives local information on the electron temperature of the emitting electrons. This interrelation is particularly useful because the cyclotron radiation reaches, under conditions fulfilled in the majority of cases, the blackbody level, so that the radiation temperature reaches the physical temperature of the emitting electrons. Wave propagation through the magnetized plasma and the physics basis of the various microwave diagnostic methods and their experimental and technological aspects are examined in detail in this book.

Microwave diagnostics fulfill the general diagnostic requirements formulated before, to a great extent. They probe the plasma without material contact. The waves used to probe are not disturbing the plasma at all, and the systems launching the waves and the ones receiving them can be positioned relatively far away from the plasma column that radiation emission and particle ejection from the plasma will not severely affect them. The plasma-facing optical components such as mirrors or horn antennas used in the millimeter-wave range can in particular be built to withstand the high radiation flux and particle impact from future burning plasma experiments without significant degradation, making them well suited as robust diagnostic systems for a few of the most important physical parameters of the hot plasma in also the next generation of fusion experiments.

Exercises

1.1 In the center of the Sun, each second, 567×10^9 kg of hydrogen are burned into 563×10^9 kg of helium. The power corresponding to the mass loss is radiated isotropically. Calculate the solar constant, the power flux in units of watts per square meter on the Earth.

1.2 The Sun is radiating like a blackbody of temperature $T = 5800$ K. Calculate with Planck's law, $I_\omega = (\omega^2/8\pi^3 c^2)/(\hbar\omega/e^{\hbar\omega/k_B T} - 1)$, the frequency ω_m of maximum emission per unit frequency. Calculate as well the wavelength λ_m of maximum emission per wavelength interval from an equivalent expression I_λ, giving the emission per unit wavelength.

1.3 Why are the two not connected through $\lambda_m \omega_m = 2\pi c$?

1.4 Formulate Wien's displacement law, $\lambda_m T = 2.898 \times 10^{-3}$ mK for frequencies.

1.5 In DT-fusion, the total energy released is 17.6 MeV. Verify that the energy is distributed onto the reaction products, as given in Equation 1.2.

1.6 If a straight solenoidal coil, with the current flowing in it generating a certain magnetic induction, is bend to a torus, the homogeneous axial field is deformed into an axisymmetric toroidal field. Show that the toroidal field has

a maximum on its inner side decaying along the major torus radius R. Derive the field gradient as function of radius.

1.7 What is the average time an electron and a proton need to orbit around the torus at $R = 2$ m? The plasma temperature is $T = T_e = T_i$ with $k_B T = 1$ keV. With the parallel toroidal direction representing one degree of freedom, the average parallel kinetic energy is $(1/2)m\langle v_{||}^2\rangle = (1/2)k_B T_e$, $v_{||}^2 = v_z^2$. What is the perpendicular kinetic energy $(1/2)m\langle v_\perp^2\rangle$ with $v_\perp^2 = v_x^2 + v_y^2$ expressed by the temperature? What is the ratio of perpendicular-to-parallel kinetic energy for an isotropic plasma with $T_{||} = T_\perp$?

References

1. (a) Alpher, R.A., Bethe, H.A., and Gamow, G. (1948) *Phys. Rev.*, **73**, 803. (b) Clayton, D.D. (1968) *Principles of Stellar Evolution and Nucleosynthesis*, McGraw-Hill, New York: reissued by (1983) University of Chicago Press.
2. Adelberger, E.C. *et al.* (2011) *Rev. Mod. Phys.*, **83**, 195.
3. Chen, F.F. (2011) *An Indispensable Truth*, Springer, New York, Dordrecht, Heidelberg, London.
4. Boozer, A.H. (2004) *Rev. Mod. Phys.*, **76**, 1071.
5. Stacey, W.M. (2012) *Fusion Plasma Physics*, 2nd edn, Wiley-VCH Verlag GmbH, Weinheim.
6. Lackner, K. *et al.* (2012) Equilibrium and macroscopic stability of tokamaks, in *Fusion Physics* (eds M. Kikuchi, K. Lackner, and M.Q. Tran), International Atomic Energy Agency, Vienna.
7. Beidler, C. *et al.* (2012) Helical confinement concepts, in *Fusion Physics* (eds M. Kikuchi, K. Lackner, and M.Q. Tran), International Atomic Energy Agency, Vienna.
8. Wagner, F. (2013) Fusion energy by magnetic confinement, in *Encyclopedia of Nuclear Physics and Its Applications* (ed R. Stock), Wiley-VCH Verlag GmbH, Weinheim.
9. Shimada, M. *et al.* (2007) Progress in the ITER physics basis. *Nucl. Fusion*, **47**, S1.
10. Goldston, R. *et al.* (2012) Physics of confinement, in *Fusion Physics* (eds M. Kikuchi, K. Lackner, and M.Q. Tran), International Atomic Energy Agency, Vienna.
11. Li, J. *et al.* (2012) Plasma wall interaction, in *Fusion Physics* (eds M. Kikuchi, K. Lackner, and M.Q. Tran), International Atomic Energy Agency, Vienna.
12. Lawson, J.D. (1957) *Proc. Phys. Soc. B*, **70**, 6.
13. Dinklage, A. *et al.* (2007) *Fusion Sci. Technol.*, **51**, 1.
14. Team, J.E.T. (1999) *Nucl. Fusion*, **39**, 1227.
15. Strachan, J.D. *et al.* (1994) *Plasma Phys. Controlled Fusion*, **36**, B3.
16. Kikuchi, M. and Okumara, Y. (2012) Plasma heating and current drive by neutral beam and alpha particles, in *Fusion Physics* (eds M. Kikuchi, K. Lackner, and M.Q. Tran), International Atomic Energy Agency, Vienna.
17. Porkolab, M. *et al.* (2012) Radiofrequency waves, heating and current drive in magnetically confined plasmas, in *Fusion Physics* (eds M. Kikuchi, K. Lackner, and M.Q. Tran), International Atomic Energy Agency, Vienna.
18. Dinklage, A. *et al.* (2008) in *Burning Plasma Diagnostics*, AIP Conference Proceedings, vol. 988 (eds F.P. Orsitto, G. Gorini, E. Sindoni, and M. Tardocchi), American Institute of Physics Inc., New York, p. 471.
19. Hutchinson, I.H. (2002) *Principles of Plasma Diagnostics*, 2nd edn, Cambridge University Press, Cambridge.
20. Lochte-Holtgreven, W. (1995) Plasma diagnostics, in *American Vacuum Society Classics* (ed. H.F. Dylla), AIP Press, New York (Originally published in 1968 by North-Holland Publishing Company).